



CERN-EP-2022-277
LHCb-PAPER-2022-046
December 20, 2022

Test of lepton universality in $b \rightarrow s \ell^+ \ell^-$ decays

LHCb collaboration

Abstract

The first simultaneous test of muon-electron universality using $B^+ \rightarrow K^+ \ell^+ \ell^-$ and $B^0 \rightarrow K^{*0} \ell^+ \ell^-$ decays is performed, in two ranges of the dilepton invariant-mass squared, q^2 . The analysis uses beauty mesons produced in proton-proton collisions collected with the LHCb detector between 2011 and 2018, corresponding to an integrated luminosity of 9 fb^{-1} . Each of the four lepton universality measurements reported is either the first in the given q^2 interval or supersedes previous LHCb measurements. The results are compatible with the predictions of the Standard Model.

Submitted to Phys. Rev. Lett.

Within the Standard Model of particle physics (SM), Lepton Universality (LU) states that the electroweak gauge bosons couple equally to all three families of leptons. Although LU is not protected by a fundamental conservation law in the SM, it has been validated experimentally at the percent and per mille levels in the decays of W and Z bosons, respectively [1–13]. New particles in extensions of the SM may violate this symmetry, resulting in observable changes for the rates of quark-lepton transitions in the decays of SM hadrons.

In this context, rare, “nonresonant” semileptonic $b \rightarrow s\ell^+\ell^-$ decays, where ℓ represents either an electron or a muon, are particularly interesting [14, 15]. The contribution of different operators to the SM decay rate varies as a function of the square of the dilepton invariant mass, q^2 . In the SM, differences in the decay rates to electron and muon final states originate solely from lepton mass effects and are below the per mille level across the vast majority of final states and q^2 regions. Modeling of final state radiation is the dominant source of uncertainty in the SM prediction of the observable difference between the electron and muon decay rates in $b \rightarrow s\ell^+\ell^-$ processes, and there is consensus that this uncertainty is at most 1% [16–18]. In contrast, models extending the SM can introduce violation of LU in these transitions by more than 10% while remaining compatible with all other experimental constraints [19–26]. Hence, any observed violation of LU in $b \rightarrow s\ell^+\ell^-$ decays would be an unambiguous sign of physics beyond the SM. Using current experimental data, these decays are sensitive to the existence of particles beyond the SM at energy scales up to $\mathcal{O}(50 \text{ TeV})$ [27].

In recent years there has been an accumulation of LU measurements in $b \rightarrow s\ell^+\ell^-$ transitions [28–37] showing a coherent pattern of deviations from the predictions of the SM. Notably, the most recent LHCb LU test using $B^+ \rightarrow K^+\ell^+\ell^-$ decays [32] reported evidence for violation of LU with a significance of 3.1σ and a combined statistical and systematic uncertainty of around 5%. In addition, measurements of angular observables and decay rates in $b \rightarrow s\mu^+\mu^-$ decays have also shown a similarly intriguing pattern of deviations from SM predictions [38–49]. A wide variety of phenomenological models has been proposed to explain these measurements, *e.g.* Refs. [19–26], with many predicting the existence of observable TeV-scale particles. It is therefore imperative to obtain a full understanding of the possible size of LU effects in $b \rightarrow s\ell^+\ell^-$ transitions.

This Letter reports the first simultaneous test of muon-electron universality in non-resonant $B^+ \rightarrow K^+\ell^+\ell^-$ and $B^0 \rightarrow K^{*0}\ell^+\ell^-$ decays that adopts a coherent approach to experimental effects, including cross-feed between different channels. A more comprehensive description of this test is reported in a companion article [50]. The inclusion of charge-conjugated processes is implied throughout the Letter. The $K^*(892)^0$ meson, denoted hereafter by K^{*0} , is reconstructed in the $K^+\pi^-$ final state within $100 \text{ MeV}/c^2$ of its known mass [51]. The observables R_K and R_{K^*} are defined in terms of the decay rates Γ as

$$R_{(K,K^*)}(q_a^2, q_b^2) = \frac{\int_{q_a^2}^{q_b^2} \frac{d\Gamma(B^{(+,0)} \rightarrow K^{(+,*0)}\mu^+\mu^-)}{dq^2} dq^2}{\int_{q_a^2}^{q_b^2} \frac{d\Gamma(B^{(+,0)} \rightarrow K^{(+,*0)}e^+e^-)}{dq^2} dq^2}, \quad (1)$$

and measured in two q^2 intervals: $0.1 < q^2 < 1.1 \text{ GeV}^2/c^4$, referred to as low- q^2 , and $1.1 < q^2 < 6.0 \text{ GeV}^2/c^4$ referred to as central- q^2 . All pp collision data recorded using the

LHCb detector between 2011 and 2018 are used, corresponding to integrated luminosities of 1.0, 2.0, and 6.0 fb⁻¹ at center-of-mass energies of 7, 8, and 13 TeV, respectively. In addition to the nonresonant decays in the low- q^2 and central- q^2 intervals, “resonant” $B^{(+,0)} \rightarrow K^{(+,*0)} J/\psi (\rightarrow \ell^+ \ell^-)$ and $B^{(+,0)} \rightarrow K^{(+,*0)} \psi(2S) (\rightarrow \ell^+ \ell^-)$ decays are selected by requiring $6 < q^2 < 11 \text{ GeV}^2/c^4$ and $11 < q^2 < 15 \text{ GeV}^2/c^4$, respectively, for electrons and by taking $\sqrt{q^2}$ within 100 MeV/ c^2 of the known J/ψ or $\psi(2S)$ [51] mass for muons. These resonant decays are used both to calibrate the analysis and to reduce biases induced by differences in the detector response for electrons and muons.

Selection procedures for the $K^+ e^+ e^-$, $K^+ \mu^+ \mu^-$, $K^+ \pi^- e^+ e^-$ and $K^+ \pi^- \mu^+ \mu^-$ final states of B^0 and B^+ decays are harmonised to make the calibration of efficiencies as robust as possible. This maximises the cancellation of efficiencies between the four processes in the final LU observables which, following previous analyses, are measured as double ratios,

$$R_{(K,K^*)} \equiv \frac{\frac{N}{\epsilon}(B^{(+,0)} \rightarrow K^{(+,*0)} \mu^+ \mu^-)}{\frac{N}{\epsilon}(B^{(+,0)} \rightarrow K^{(+,*0)} J/\psi (\rightarrow \mu^+ \mu^-))} \bigg/ \frac{\frac{N}{\epsilon}(B^{(+,0)} \rightarrow K^{(+,*0)} e^+ e^-)}{\frac{N}{\epsilon}(B^{(+,0)} \rightarrow K^{(+,*0)} J/\psi (\rightarrow e^+ e^-))}, \quad (2)$$

where $\frac{N}{\epsilon}(X)$ represents the efficiency corrected yield for process X . These detector efficiencies are calibrated using resonant $B^{(+,0)} \rightarrow K^{(+,*0)} J/\psi (\rightarrow \ell^+ \ell^-)$ decays; the calibrations derived using K^+ and K^{*0} final states are shown to be interchangeable for the first time. The measurements of R_K and R_{K^*} are optimized for statistical precision. This leads to stringent particle identification (PID) requirements and dedicated multivariate selections to suppress backgrounds from hadronic and partially reconstructed b -hadron decays, and a higher purity than previous LHCb analyses of these final states [29, 32]. Finally, data are used for the first time to measure residual backgrounds from misidentified b -hadron decays for the final measurement of the $R_{(K,K^*)}$ observables. These choices improve the statistical sensitivity per unit integrated luminosity and allow systematic uncertainties to be estimated more reliably than in previous LHCb analyses of the same final states.

The LHCb detector [52, 53] is a single-arm forward spectrometer covering the pseudorapidity range $2 < \eta < 5$. Simulated events produced with the software described in Refs. [54–56] are used to model the effects of the detector acceptance, resolution, and the imposed selection requirements. Dedicated simulated samples are produced for each year of data taking corresponding to the relevant detector and accelerator conditions. Final-state radiation is generated using PHOTOS [57]. Samples of charm hadron, charmonia, and beauty hadron decays are collected for all data-taking periods and are used to calibrate the simulated single-particle reconstruction and PID efficiencies, ensuring that they match the performance of the detector. The real-time selection of LHC bunch crossings (events) is performed by a trigger [58], which consists of a hardware stage, based on information from the calorimeter and muon systems, followed by a software stage, which applies a full event reconstruction. At the hardware trigger stage, events with large detector occupancy are rejected and the remaining events are required to have a muon with high transverse momentum relative to the beamline (p_T), or a hadron or an electron with high transverse energy in the calorimeters. The software trigger requires a two- or three-body secondary vertex with significant displacement from any primary pp interaction vertex. At least one charged particle must have significant p_T and be inconsistent with originating from a primary vertex. A multivariate algorithm [59, 60] based on kinematic, geometric and lepton identification criteria is used for the identification of secondary vertices consistent with the decay of a b hadron.

Signal candidates are reconstructed by combining two oppositely charged electrons or muons with either a K^+ or K^{*0} meson candidate. Calorimeter clusters are identified as bremsstrahlung associated with electron candidates if they are consistent with a straight-line extrapolation of the electron candidate's trajectory from the bremsstrahlung emission point.

All final-state particles are required to be within the geometric acceptance of the PID systems (RICH, calorimeters and muon detectors [53]) and the momentum range covered by the PID calibration samples. They are also required to satisfy minimum p_T requirements and to have significant displacement from the primary pp collision associated with the signal candidate. A combination of requirements on individual PID systems and multivariate classifiers, which combine information from all PID systems, is used to identify the final state particles. Identical PID requirements are used in all q^2 ranges.

Two groups of multivariate classifiers, designed to be as similar as possible in their choice of features between the B^+ and B^0 signal decays, are used to separate signal from residual backgrounds. The first group of classifiers is trained to separate simulated signal from random combinatorial backgrounds using kinematic and geometric features of the final-state particles and the signal candidate vertex, as well as the vertex fit quality. Candidates passing all other selection requirements and having an invariant mass greater than 5400 (5600) MeV/c^2 are used as a proxy for background when training the first muon (electron) classifiers. A k -folding approach [61] is used to avoid bias. The second group of classifiers is trained to separate signal from the partially reconstructed b -hadron decays $B \rightarrow (K, K^{*0})\ell^+\ell^-X$, where X represents one or more additional hadrons. Kinematic and geometric features of the signal candidate are used, as well as features describing the spatial and kinematic isolation of the final-state particles and the signal candidate from other reconstructed particles. Although a limited number of simulated backgrounds with a single missing pion are used for training, the classifiers have significant discrimination against most partially reconstructed decays.

The working points of the two groups of classifiers are optimized simultaneously, using the expected signal significance for the predicted SM decay rates as the figure of merit. The optimal working point is chosen separately for each signal mode, q^2 region, lepton flavor, and data-taking period. For the electron mode, the ratio of the hadronic and dielectron momentum components transverse to the B -meson flight direction are used to correct the momentum of the dielectron pair [29]. The resulting corrected mass has significant power to separate signal from partially reconstructed backgrounds and is therefore used in the analysis, with the working point chosen analogously to the process followed for the multivariate classifiers. As in previous LHCb LU tests [29, 32], dedicated simulated event samples are used to study backgrounds that remain after all selection criteria have been applied. Specific vetoes are used to eliminate backgrounds resulting from misidentified $B \rightarrow D(\rightarrow K\pi)e\nu_e$ and $B \rightarrow D(\rightarrow K e\nu_e)\pi$ decays. Resonant $B^{(+,0)} \rightarrow K^{(+,*0)}J/\psi(\rightarrow \ell^+\ell^-)$ and $B^{(+,0)} \rightarrow K^{(+,*0)}\psi(2S)(\rightarrow \ell^+\ell^-)$ decays in which a hadron and lepton of the same charge are swapped are similarly vetoed. Finally, electron candidates are divided into three categories according to the number of bremsstrahlung photons (0, 1, > 1) associated with the final-state e^+e^- pair. After the application of all criteria, there are no nonresonant signal candidates in common between the B^0 and B^+ samples. Around one percent of selected events have multiple candidates; in such cases a single reconstructed candidate is chosen randomly.

The LHCb detector simulation is calibrated to ensure an accurate description of

differences in detector response for electrons and muons. This is performed using an iterative multi-step process, where the output of each step a is a set of weights w_a characterizing the relative efficiency of data and simulation as a function of the signal candidate kinematics. Several of these steps use the same $B^{(+,0)} \rightarrow K^{(+,*0)} J/\psi (\rightarrow \ell^+ \ell^-)$ resonant decays that are subsequently used in the analysis itself. The weights are therefore computed for both B^0 and B^+ decays and shown to be interchangeable. To minimize correlations between the calibration samples and the candidates used in the final analysis, weights derived from B^0 samples are used to correct B^+ efficiencies and vice versa.

Data calibration samples are used to evaluate PID efficiencies for hadrons, muons, and electrons as a function of particle momentum, pseudorapidity and the detector occupancy. Electron identification efficiencies are also evaluated separately for candidates having one or no associated bremsstrahlung photons. Simulation is used to verify that PID requirements factorize, so that the derived data-simulation weights w_{PID} can be applied independently of one another. Hadron and muon particle identification efficiencies are found to factorize, whereas for electrons with overlapping calorimeter clusters the efficiencies depend strongly on both q^2 and the separation of the electron trajectories extrapolated to the calorimeter. The electron and positron candidates are required to be well separated on entering the calorimeters. Particle reconstruction efficiencies are found to factorize for all particle species. Muon and hadron reconstruction efficiencies are found to be described well by simulation and do not require calibration, while electron reconstruction efficiencies are calibrated using weights w_{TRK} in intervals of momentum, pseudorapidity and in two geometric regions of the vertex detector that encode the amount of material traversed by the electron.

The kinematics of the B meson and the multiplicity of the underlying event are calibrated using weights $w_{\text{Mult\&Kin}}$ by training a boosted decision tree (BDT) [62] with the `hep_ml` library [63]. The event track multiplicity and the signal candidate p_{T} , momentum and pseudorapidity are used as inputs. The BDT is trained using $B^{(+,0)} \rightarrow K^{(+,*0)} J/\psi (\rightarrow \mu^+ \mu^-)$ candidates selected in data and using a specific trigger path that is fully aligned between data and simulation in all data-taking periods. The hardware trigger efficiencies are calibrated using weights w_{L0} as a function of muon p_{T} and electron transverse energy, while the software trigger efficiencies are calibrated using weights w_{HLT} as a function of event track multiplicity. Finally, residual data-simulation differences are corrected by weights w_{Reco} from a second BDT, trained using the same kinematic variables as the first BDT and the χ^2_{IP} of the B and J/ψ mesons, with χ^2_{IP} defined as the difference in χ^2 of the primary pp collision vertex with and without the considered particle.

The invariant-mass resolution of the simulated electron data must also be calibrated using weights w_{Res} so that the migration of candidates between q^2 regions can be evaluated accurately. This calibration is derived by fitting the dielectron invariant mass component of the fully selected resonant $B^{(+,0)} \rightarrow K^{(+,*0)} J/\psi (\rightarrow e^+ e^-)$ candidates in data and simulation. A modified Crystal Ball function [64] with power-law tails both above and below the mean mass value is used to model the dielectron spectrum, with the remaining combinatorial background modeled using an exponential function.

Four efficiency corrected resonant mode yield ratios are defined as benchmarks for this analysis: $r_{J/\psi}^K$ and $R_{\psi(2S)}^K$ using B^+ candidates; $r_{J/\psi}^{K*}$ and $R_{\psi(2S)}^{K*}$ using B^0 candidates. The single ratios $r_{J/\psi}^K$ and $r_{J/\psi}^{K*}$ represent the yields of $B^{(+,0)} \rightarrow K^{(+,*0)} J/\psi (\rightarrow \mu^+ \mu^-)$ decays relative to $B^{(+,0)} \rightarrow K^{(+,*0)} J/\psi (\rightarrow e^+ e^-)$ decays. The double ratios $R_{\psi(2S)}^K$ and $R_{\psi(2S)}^{K*}$ are

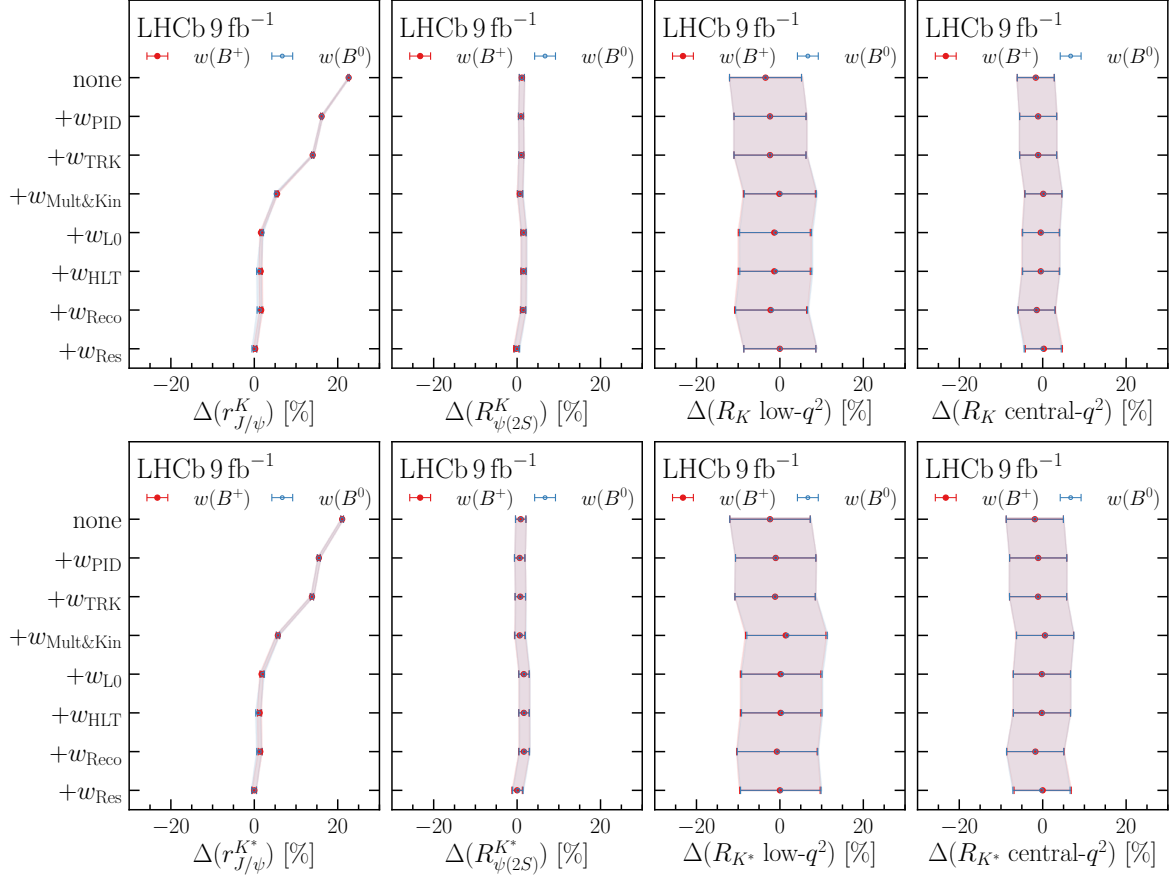


Figure 1: Variation of efficiency corrected ratios (top row, left to right): $r_{J/\psi}^K$, $R_{\psi(2S)}^K$, R_K in low- and central- q^2 regions; (bottom row) analogous plots for the K^{*0} channel. Measurements are relative to the final value for the given observable. The simulation calibration using B^0 and B^+ chains for successive calibration weights are shown and almost indistinguishable.

analogous to Eq. 2 but with $B^{(+,0)} \rightarrow K^{(+,*0)}\psi(2S)(\rightarrow \ell^+\ell^-)$ in place of the nonresonant $B^{(+,0)} \rightarrow K^{(+,*0)}\ell^+\ell^-$ decays. Resonant mode yields are extracted using a simultaneous maximum-likelihood fit to the invariant mass of the B candidate. Signal lineshapes, as well as misidentified and partially reconstructed background shapes, are derived using simulated data. Residual data-simulation differences are parametrized by a shift in the mean and a scale factor applied to the width of the signal lineshape. Remaining combinatorial backgrounds are modeled using an exponential function with a freely varying slope. Ratios of misidentified background yields are constrained between the electron and muon final states using efficiencies derived from simulated data. The measured single ratios are found to be $r_{J/\psi}^K = 1.047 \pm 0.024$ and $r_{J/\psi}^{K*} = 1.028 \pm 0.024$, while the measured double ratios are found to be $R_{\psi(2S)}^K = 0.987 \pm 0.007$ and $R_{\psi(2S)}^{K*} = 1.012 \pm 0.013$. These uncertainties include both statistical and systematic components: the latter dominate for the single ratios, while the opposite is true for the double ratios. The $r_{J/\psi}^K$ and $r_{J/\psi}^{K*}$ ratios have no significant dependence on kinematic and geometrical quantities, and a systematic uncertainty is assigned for residual non-flatness. As in previous LHCb lepton universality tests, agreement of these quantities with predictions of the SM was a prerequisite to evaluating the $R_{(K,K^*)}$ observables.

Figure 1 illustrates the evolution of the efficiency corrected ratios $r_{J/\psi}^K$, $r_{J/\psi}^{K*}$, $R_{\psi(2S)}^K$ and $R_{\psi(2S)}^{K*}$ as a function of the corrections applied to the simulated data. Since measurements of these resonant decays are consistent with LU [51], they are excellent control modes for this analysis. Although the B^0 and B^+ weights are found to be interchangeable, the 25% effect observed in the efficiency corrected single ratios leads to undesirably large systematic uncertainties. These are reduced by defining the final observables using the double ratio of Eq. 2.

Figure 1 also shows the evolution of this double ratio for each of the two observables and q^2 ranges. Contrary to the single ratio, the impact of the calibration chain on the double ratio is less than a few percent, significantly reducing systematic uncertainties associated with the determination of efficiencies from simulated data. The double ratio is evaluated using a simultaneous maximum-likelihood fit to the B^+ and B^0 candidate invariant masses in the low- q^2 , central- q^2 and J/ψ regions, where the efficiencies are constrained using values and uncertainties obtained from simulated data.

After all selection criteria have been applied, the nonresonant muon candidate samples contain only signal and combinatorial backgrounds. The invariant mass spectrum of the nonresonant muon signals is modeled using simulated data, while the combinatorial background is modeled using an exponential function with a freely varying slope. Small adjustments to the mean and width of the signal distribution are constrained to be the same as for the resonant muon signal. The normalization of both components is allowed to vary freely.

The nonresonant electron candidate samples have a more complex composition. In addition to signal and combinatorial background they contain: resonant J/ψ meson decays that migrate into the central- q^2 (but not low- q^2) region (“leakage”); partially reconstructed decays without misidentification; residual misidentified hadronic decays. The invariant mass spectra of the nonresonant electron signals are modeled following a similar procedure to the muon modes and over a wider mass range than previous analyses, reducing correlations between components. The combinatorial background is modeled using an exponential function with freely varying normalization multiplied by a function that parametrizes the distortion by the corrected mass and partially reconstructed selection criteria. The parameters of this function are fixed from background data reconstructed using two leptons of the same charge and varied in pseudoexperiments to attribute an associated systematic uncertainty. The leakage is modeled using a kernel-density estimator [65] derived from simulated data; its normalization is constrained to the observed resonant mode yields multiplied by efficiencies measured in simulation. The partially reconstructed backgrounds are modeled using kernel-density estimators derived from simulated data, with a systematic uncertainty assigned for the finite number of different partially reconstructed decays that are simulated. Their normalization is allowed to vary freely for the B^0 nonresonant candidate samples. In the B^+ samples, the normalization is constrained to the observed nonresonant B^0 signal yields in the same q^2 region multiplied by efficiencies measured in simulation and accounting for isospin partner modes.

Residual misidentified backgrounds may contain one or two hadrons misidentified as electrons, as well as additional missing energy. A wide range of these backgrounds are studied using simulated data and each individual background is found to be small compared to the expected statistical sensitivity. However, the large number of potential hadronic B decays, which in many cases have poorly known or unknown dynamics, means that their overall contribution to the final candidate sample is not necessarily small.

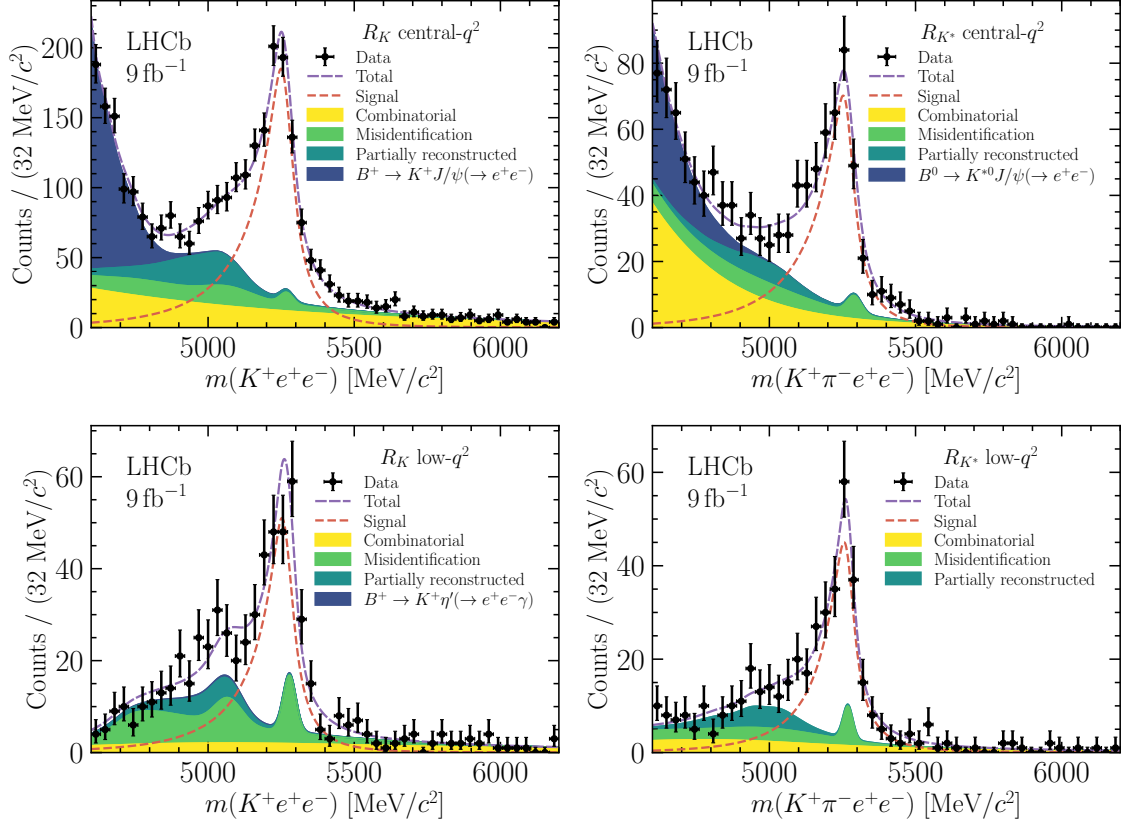


Figure 2: Invariant mass distributions of the nonresonant (left) $B^+ \rightarrow K^+ e^+ e^-$ and (right) $B^0 \rightarrow K^{*0} e^+ e^-$ candidates in (upper) central- q^2 and (lower) low- q^2 regions. The results of the fit described in the text are also presented.

Data are therefore used to estimate the overall invariant mass spectra and normalization of such backgrounds. A sample enriched with background from misidentification of nonresonant candidates is defined for each of the four LU observables by inverting the electron identification criteria and using less stringent electron identification requirements. This sample is corrected for the residual contribution of signal decays and then weighted using misidentification rates measured from data to obtain the expected misidentified backgrounds that would pass all selection criteria. The invariant mass shape of these backgrounds is modeled using an empirical function; their normalization is constrained using the measured central values and uncertainties.

The invariant mass distributions of the nonresonant electron candidates resulting from the final fit to the four LU observables are shown in Fig. 2. The measured values of the observables of interest are

$$\begin{aligned} \text{low-}q^2 \begin{cases} R_K &= 0.994^{+0.090}_{-0.082} (\text{stat})^{+0.029}_{-0.027} (\text{syst}), \\ R_{K^*} &= 0.927^{+0.093}_{-0.087} (\text{stat})^{+0.036}_{-0.035} (\text{syst}), \end{cases} \\ \text{central-}q^2 \begin{cases} R_K &= 0.949^{+0.042}_{-0.041} (\text{stat})^{+0.022}_{-0.022} (\text{syst}), \\ R_{K^*} &= 1.027^{+0.072}_{-0.068} (\text{stat})^{+0.027}_{-0.026} (\text{syst}). \end{cases} \end{aligned}$$

All four measurements are in agreement with predictions of the SM [16, 17, 66–74].

Systematic uncertainties associated with efficiencies are evaluated by varying the assumptions made when calibrating the simulated samples. The biggest uncertainty of this type is the stability of the $r_{J/\psi}^K$ and $r_{J/\psi}^{K^*}$ ratios as a function of different kinematic and geometric variables associated with these decays. The overall systematic uncertainties for efficiencies are below 1% in all cases except R_{K^*} low- q^2 where they are 2%. Systematic uncertainties associated with the modeling of nonresonant decay form factors, which affect the efficiencies, are evaluated using simulation and found to be negligible for B^+ decays and around 1% for B^0 decays. Systematic uncertainties associated with the modeling of the invariant mass distributions are dominated by the data-driven modeling of misidentified backgrounds, and are 2.0–2.5% depending on the LU observable in question. Although larger than the systematic uncertainties assigned in the previous LHCb analyses [29, 32], these are significantly smaller than the statistical uncertainties associated with each of the four LU observables.

The results presented here differ from previous LHCb measurements of R_K [32] and R_{K^*} [29]. For R_K central- q^2 , the difference is partly due to the use of tighter electron identification criteria and partly due to the modeling of the residual misidentified hadronic backgrounds; statistical fluctuations make a smaller contribution to the difference since the same data are used as in Ref. [32]. The systematic shift due to misidentified hadronic backgrounds consists of components related to the tighter PID working point (0.064) and the treatment of the residual component in the fit (0.038). The statistical component of the difference has been evaluated using pseudoexperiments and found to have a Gaussian distribution of width 0.033.

The measurements of R_K and R_{K^*} for the q^2 intervals $0.1 < q^2 < 1.1 \text{ GeV}^2/c^4$ and $1.1 < q^2 < 6.0 \text{ GeV}^2/c^4$ reported here supersede previous LHCb measurements [29, 32] and are in agreement with the predictions of the SM. The systematic uncertainties associated with these measurements remain significantly smaller than the statistical uncertainties and are expected to reduce further with more data.

References

- [1] UA1 collaboration, C. Albajar *et al.*, *Studies of intermediate vector boson production and decay in UA1 at the CERN Proton-Antiproton Collider*, Z. Phys. **C44** (1989) 15.
- [2] CDF collaboration, F. Abe *et al.*, *Measurement of the ratio $B(W \rightarrow \tau\nu)/B(W \rightarrow e\nu)$, in $p\bar{p}$ collisions at $\sqrt{s} = 1.8 \text{ TeV}$* , Phys. Rev. Lett. **68** (1992) 3398.
- [3] UA2 collaboration, J. Alitti *et al.*, *A search for charged Higgs from top quark decay at the CERN $\bar{p}p$ collider*, Phys. Lett. **B280** (1992) 137.
- [4] CDF collaboration, F. Abe *et al.*, *A measurement of the production and muonic decay rate of W and Z bosons in $p\bar{p}$ collisions at $\sqrt{s} = 1.8 \text{ TeV}$* , Phys. Rev. Lett. **69** (1992) 28.
- [5] D0 collaboration, S. Abachi *et al.*, *W and Z boson production in $p\bar{p}$ collisions at $\sqrt{s} = 1.8 \text{ TeV}$* , Phys. Rev. Lett. **75** (1995) 1456, [arXiv:hep-ex/9505013](#).

- [6] D0 collaboration, B. Abbott *et al.*, *A measurement of the $W \rightarrow \tau\nu$ production cross-section in $p\bar{p}$ collisions at $\sqrt{s} = 1.8$ TeV*, Phys. Rev. Lett. **84** (2000) 5710, [arXiv:hep-ex/9912065](#).
- [7] ALEPH, DELPHI, L3, OPAL, SLD, LEP Electroweak Working Group, SLD Electroweak Group, SLD Heavy Flavour Group, S. Schael *et al.*, *Precision electroweak measurements on the Z resonance*, Phys. Rept. **427** (2006) 257, [arXiv:hep-ex/0509008](#).
- [8] ALEPH, DELPHI, L3, OPAL, LEP Electroweak collaboration, S. Schael *et al.*, *Electroweak measurements in electron-positron collisions at W-boson-pair energies at LEP*, Phys. Rept. **532** (2013) 119, [arXiv:1302.3415](#).
- [9] ATLAS collaboration, M. Aaboud *et al.*, *Precision measurement and interpretation of inclusive W^+ , W^- and Z/γ^* production cross sections with the ATLAS detector*, Eur. Phys. J. **C77** (2017) 367, [arXiv:1612.03016](#).
- [10] ATLAS collaboration, G. Aad *et al.*, *Test of the universality of τ and μ lepton couplings in W-boson decays with the ATLAS detector*, Nature Phys. **17** (2021) 813, [arXiv:2007.14040](#).
- [11] CMS collaboration, A. Tumasyan *et al.*, *Precision measurement of the W boson decay branching fractions in proton-proton collisions at $\sqrt{s} = 13$ TeV*, Phys. Rev. D **105** (2022) 072008, [arXiv:2201.07861](#).
- [12] LHCb collaboration, R. Aaij *et al.*, *Measurement of forward $W \rightarrow e\nu$ production in pp collisions at $\sqrt{s} = 8$ TeV*, JHEP **10** (2016) 030, [arXiv:1608.01484](#).
- [13] LHCb collaboration, R. Aaij *et al.*, *Measurement of $Z \rightarrow \tau^+\tau^-$ production in proton-proton collisions at $\sqrt{s} = 8$ TeV*, JHEP **09** (2018) 159, [arXiv:1806.05008](#).
- [14] Y. Wang and D. Atwood, *Rate difference between $b \rightarrow s\mu^+\mu^-$ and $b \rightarrow se^+e^-$ in supersymmetry with large $\tan\beta$* , Phys. Rev. **D68** (2003) 094016, [arXiv:hep-ph/0304248](#).
- [15] G. Hiller and F. Krüger, *More model-independent analysis of $b \rightarrow s$ processes*, Phys. Rev. **D69** (2004) 074020, [arXiv:hep-ph/0310219](#).
- [16] M. Bordone, G. Isidori, and A. Pattori, *On the Standard Model predictions for R_K and R_{K^*}* , Eur. Phys. J. **C76** (2016) 440, [arXiv:1605.07633](#).
- [17] G. Isidori, S. Nabeebaccus, and R. Zwicky, *QED corrections in $\bar{B} \rightarrow \bar{K}\ell^+\ell^-$ at the double-differential level*, JHEP **12** (2020) 104, [arXiv:2009.00929](#).
- [18] G. Isidori, D. Lancierini, S. Nabeebaccus, and R. Zwicky, *QED in $\bar{B} \rightarrow \bar{K}\ell^+\ell^-$ LFU ratios: theory versus experiment, a Monte Carlo study*, JHEP **10** (2022) 146, [arXiv:2205.08635](#).
- [19] G. Hiller and M. Schmaltz, *R_K and future $b \rightarrow s\ell\ell$ physics beyond the standard model opportunities*, Phys. Rev. **D90** (2014) 054014, [arXiv:1408.1627](#).
- [20] B. Gripaios, M. Nardecchia, and S. A. Renner, *Composite leptoquarks and anomalies in B-meson decays*, JHEP **05** (2015) 006, [arXiv:1412.1791](#).

- [21] I. de Medeiros Varzielas and G. Hiller, *Clues for flavor from rare lepton and quark decays*, JHEP **06** (2015) 072, [arXiv:1503.01084](#).
- [22] R. Barbieri, C. W. Murphy, and F. Senia, *B-decay anomalies in a composite leptoquark model*, Eur. Phys. J. **C77** (2017) 8, [arXiv:1611.04930](#).
- [23] W. Altmannshofer, S. Gori, M. Pospelov, and I. Yavin, *Quark flavor transitions in $L_\mu - L_\tau$ models*, Phys. Rev. **D89** (2014) 095033, [arXiv:1403.1269](#).
- [24] A. Crivellin, G. D’Ambrosio, and J. Heeck, *Explaining $h \rightarrow \mu^\pm \tau^\mp$, $B \rightarrow K^* \mu^+ \mu^-$ and $B \rightarrow K \mu^+ \mu^- / B \rightarrow K e^+ e^-$ in a two-Higgs-doublet model with gauged $L_\mu - L_\tau$* , Phys. Rev. Lett. **114** (2015) 151801, [arXiv:1501.00993](#).
- [25] A. Celis, J. Fuentes-Martin, M. Jung, and H. Serodio, *Family nonuniversal Z' models with protected flavor-changing interactions*, Phys. Rev. **D92** (2015) 015007, [arXiv:1505.03079](#).
- [26] A. Falkowski, M. Nardecchia, and R. Ziegler, *Lepton flavor non-universality in B-meson decays from a $U(2)$ flavor model*, JHEP **11** (2015) 173, [arXiv:1509.01249](#).
- [27] LHCb collaboration, *Physics case for an LHCb Upgrade II — Opportunities in flavour physics, and beyond, in the HL-LHC era*, [arXiv:1808.08865](#).
- [28] LHCb collaboration, R. Aaij *et al.*, *Test of lepton universality using $B^+ \rightarrow K^+ \ell^+ \ell^-$ decays*, Phys. Rev. Lett. **113** (2014) 151601, [arXiv:1406.6482](#).
- [29] LHCb collaboration, R. Aaij *et al.*, *Test of lepton universality with $B^0 \rightarrow K^{*0} \ell^+ \ell^-$ decays*, JHEP **08** (2017) 055, [arXiv:1705.05802](#).
- [30] LHCb collaboration, R. Aaij *et al.*, *Search for lepton-universality violation in $B^+ \rightarrow K^+ \ell^+ \ell^-$ decays*, Phys. Rev. Lett. **122** (2019) 191801, [arXiv:1903.09252](#).
- [31] LHCb collaboration, R. Aaij *et al.*, *Test of lepton universality using $\Lambda_b^0 \rightarrow p K^- \ell^+ \ell^-$ decays*, JHEP **05** (2020) 040, [arXiv:1912.08139](#).
- [32] LHCb collaboration, R. Aaij *et al.*, *Test of lepton universality in beauty-quark decays*, Nature Physics **18** (2022) 277, [arXiv:2103.11769](#).
- [33] LHCb collaboration, R. Aaij *et al.*, *Tests of lepton universality using $B^0 \rightarrow K_S^0 \ell^+ \ell^-$ and $B^+ \rightarrow K^{*+} \ell^+ \ell^-$ decays*, Phys. Rev. Lett. **128** (2022) 191802, [arXiv:2110.09501](#).
- [34] Belle collaboration, S. Wehle *et al.*, *Lepton-flavor-dependent angular analysis of $B \rightarrow K^* \ell^+ \ell^-$* , Phys. Rev. Lett. **118** (2017) 111801, [arXiv:1612.05014](#).
- [35] BaBar collaboration, J. P. Lees *et al.*, *Measurement of branching fractions and rate asymmetries in the rare decays $B \rightarrow K^{(*)} \ell^+ \ell^-$* , Phys. Rev. **D86** (2012) 032012, [arXiv:1204.3933](#).
- [36] Belle collaboration, S. Choudhury *et al.*, *Test of lepton flavor universality and search for lepton flavor violation in $B \rightarrow K \ell \ell$ decays*, JHEP **03** (2021) 105, [arXiv:1908.01848](#).

- [37] Belle collaboration, A. Abdesselam *et al.*, *Test of lepton-flavor universality in $B \rightarrow K^* \ell^+ \ell^-$ decays at Belle*, Phys. Rev. Lett. **126** (2021) 161801, [arXiv:1904.02440](#).
- [38] LHCb collaboration, R. Aaij *et al.*, *Differential branching fractions and isospin asymmetries of $B \rightarrow K^{(*)} \mu^+ \mu^-$ decays*, JHEP **06** (2014) 133, [arXiv:1403.8044](#).
- [39] LHCb collaboration, R. Aaij *et al.*, *Differential branching fraction and angular analysis of $\Lambda_b^0 \rightarrow \Lambda \mu^+ \mu^-$ decays*, JHEP **06** (2015) 115, Erratum *ibid.* **09** (2018) 145, [arXiv:1503.07138](#).
- [40] LHCb collaboration, R. Aaij *et al.*, *Angular analysis and differential branching fraction of the decay $B_s^0 \rightarrow \phi \mu^+ \mu^-$* , JHEP **09** (2015) 179, [arXiv:1506.08777](#).
- [41] LHCb collaboration, R. Aaij *et al.*, *Measurements of the S-wave fraction in $B^0 \rightarrow K^+ \pi^- \mu^+ \mu^-$ decays and the $B^0 \rightarrow K^*(892)^0 \mu^+ \mu^-$ differential branching fraction*, JHEP **11** (2016) 047, Erratum *ibid.* **04** (2017) 142, [arXiv:1606.04731](#).
- [42] LHCb collaboration, R. Aaij *et al.*, *Branching fraction measurements of the rare $B_s^0 \rightarrow \phi \mu^+ \mu^-$ and $B_s^0 \rightarrow f_2'(1525) \mu^+ \mu^-$ decays*, Phys. Rev. Lett. **127** (2021) 151801, [arXiv:2105.14007](#).
- [43] LHCb collaboration, R. Aaij *et al.*, *Angular analysis of the rare decay $B_s^0 \rightarrow \phi \mu^+ \mu^-$* , JHEP **11** (2021) 043, [arXiv:2107.13428](#).
- [44] LHCb collaboration, R. Aaij *et al.*, *Angular analysis of the $B^0 \rightarrow K^{*0} \mu^+ \mu^-$ decay using 3 fb^{-1} of integrated luminosity*, JHEP **02** (2016) 104, [arXiv:1512.04442](#).
- [45] LHCb collaboration, R. Aaij *et al.*, *Measurement of CP-averaged observables in the $B^0 \rightarrow K^{*0} \mu^+ \mu^-$ decay*, Phys. Rev. Lett. **125** (2020) 011802, [arXiv:2003.04831](#).
- [46] LHCb collaboration, R. Aaij *et al.*, *Angular analysis of the $B^+ \rightarrow K^{*+} \mu^+ \mu^-$ decay*, Phys. Rev. Lett. **126** (2021) 161802, [arXiv:2012.13241](#).
- [47] ATLAS collaboration, M. Aaboud *et al.*, *Angular analysis of $B_d^0 \rightarrow K^* \mu^+ \mu^-$ decays in pp collisions at $\sqrt{s} = 8 \text{ TeV}$ with the ATLAS detector*, JHEP **10** (2018) 047, [arXiv:1805.04000](#).
- [48] CMS collaboration, V. Khachatryan *et al.*, *Angular analysis of the decay $B^0 \rightarrow K^{*0} \mu^+ \mu^-$ from pp collisions at $\sqrt{s} = 8 \text{ TeV}$* , Phys. Lett. **B753** (2016) 424, [arXiv:1507.08126](#).
- [49] CMS collaboration, A. M. Sirunyan *et al.*, *Measurement of angular parameters from the decay $B^0 \rightarrow K^{*0} \mu^+ \mu^-$ in proton-proton collisions at $\sqrt{s} = 8 \text{ TeV}$* , Phys. Lett. **B781** (2018) 517, [arXiv:1710.02846](#).
- [50] LHCb collaboration, R. Aaij *et al.*, *Measurement of lepton universality parameters in $B^+ \rightarrow K^+ \ell^+ \ell^-$ and $B^0 \rightarrow K^{*0} \ell^+ \ell^-$ decays*, LHCb-PAPER-2022-045, to be submitted to Phys. Rev. D.
- [51] Particle Data Group, R. L. Workman *et al.*, *Review of particle physics*, Prog. Theor. Exp. Phys. **2022** (2022) 083C01.

- [52] LHCb collaboration, A. A. Alves Jr. *et al.*, *The LHCb detector at the LHC*, JINST **3** (2008) S08005.
- [53] LHCb collaboration, R. Aaij *et al.*, *LHCb detector performance*, Int. J. Mod. Phys. **A30** (2015) 1530022, [arXiv:1412.6352](#).
- [54] T. Sjöstrand, S. Mrenna, and P. Skands, *A brief introduction to PYTHIA 8.1*, Comput. Phys. Commun. **178** (2008) 852, [arXiv:0710.3820](#); T. Sjöstrand, S. Mrenna, and P. Skands, *PYTHIA 6.4 physics and manual*, JHEP **05** (2006) 026, [arXiv:hep-ph/0603175](#).
- [55] I. Belyaev *et al.*, *Handling of the generation of primary events in Gauss, the LHCb simulation framework*, J. Phys. Conf. Ser. **331** (2011) 032047.
- [56] D. J. Lange, *The EvtGen particle decay simulation package*, Nucl. Instrum. Meth. **A462** (2001) 152.
- [57] N. Davidson, T. Przedzinski, and Z. Was, *PHOTOS interface in C++: Technical and physics documentation*, Comp. Phys. Comm. **199** (2016) 86, [arXiv:1011.0937](#).
- [58] R. Aaij *et al.*, *The LHCb trigger and its performance in 2011*, JINST **8** (2013) P04022, [arXiv:1211.3055](#).
- [59] V. V. Gligorov and M. Williams, *Efficient, reliable and fast high-level triggering using a bonsai boosted decision tree*, JINST **8** (2013) P02013, [arXiv:1210.6861](#).
- [60] T. Likhomanenko *et al.*, *LHCb topological trigger reoptimization*, J. Phys. Conf. Ser. **664** (2015) 082025.
- [61] A. Blum, A. Kalai, and J. Langford, *Beating the hold-out: bounds for K-fold and progressive cross-validation*, Association for Computing Machinery, New York, NY, USA, 1999.
- [62] A. Rogozhnikov, *Reweighting with Boosted Decision Trees*, J. Phys. Conf. Ser. **762** (2016) 012036, [arXiv:1608.05806](#), https://github.com/arogozhnikov/hep_ml.
- [63] A. Rogozhnikov *et al.*, *arogozhnikov/hep_ml: hep_ml v0.7.0*, doi: 10.5281/zenodo.5500612.
- [64] T. Skwarnicki, *A study of the radiative cascade transitions between the Upsilon-prime and Upsilon resonances*, PhD thesis, Institute of Nuclear Physics, Krakow, 1986, DESY-F31-86-02.
- [65] K. S. Cranmer, *Kernel estimation in high-energy physics*, Comput. Phys. Commun. **136** (2001) 198, [arXiv:hep-ex/0011057](#).
- [66] C. Bobeth, G. Hiller, and G. Piranishvili, *Angular distributions of $\bar{B} \rightarrow \bar{K} \ell^+ \ell^-$ decays*, JHEP **12** (2007) 040, [arXiv:0709.4174](#).
- [67] D. M. Straub, *flavio: a Python package for flavour and precision phenomenology in the Standard Model and beyond*, [arXiv:1810.08132](#).

- [68] D. van Dyk *et al.*, *EOS: A software for flavor physics phenomenology*, [arXiv:2111.15428](#).
- [69] B. Capdevila, S. Descotes-Genon, J. Matias, and J. Virto, *Assessing lepton-flavour non-universality from $B \rightarrow K^* \ell \ell$ angular analyses*, JHEP **10** (2016) 075, [arXiv:1605.03156](#).
- [70] B. Capdevila, S. Descotes-Genon, L. Hofer, and J. Matias, *Hadronic uncertainties in $B \rightarrow K^* \mu^+ \mu^-$: a state-of-the-art analysis*, JHEP **04** (2017) 016, [arXiv:1701.08672](#).
- [71] N. Serra, R. Silva Coutinho, and D. van Dyk, *Measuring the breaking of lepton flavor universality in $B \rightarrow K^* \ell^+ \ell^-$* , Phys. Rev. **D95** (2017) 035029, [arXiv:1610.08761](#).
- [72] W. Altmannshofer, C. Niehoff, P. Stangl, and D. M. Straub, *Status of the $B \rightarrow K^* \mu^+ \mu^-$ anomaly after Moriond 2017*, Eur. Phys. J. **C77** (2017) 377, [arXiv:1703.09189](#).
- [73] S. Jäger and J. Martin Camalich, *Reassessing the discovery potential of the $B \rightarrow K^* \ell^+ \ell^-$ decays in the large-recoil region: SM challenges and BSM opportunities*, Phys. Rev. **D93** (2016) 014028, [arXiv:1412.3183](#).
- [74] D. Ghosh, M. Nardecchia, and S. A. Renner, *Hint of lepton flavour non-universality in B meson decays*, JHEP **12** (2014) 131, [arXiv:1408.4097](#).